Chapter 2

A New Method of SHM for Steel Wire Rope and its Apparatus

Shiwei Liu, Yanhua Sun and Wenjia Ma

Additional information is available at the end of the chapter

http://dx.doi.org/10.5772/intechopen.68148

Abstract

Steel wire ropes often operate in a high-speed swing status in practical engineering, and the reliable structural health monitoring (SHM) for them directly relates to human lives; however, they are usually beyond the capability of present portable magnet magnetic flux leakage (MFL) sensors based on yoke magnetic method due to its strong magnetic force and large weight. Unlike the yoke method, a new method of SHM for steel wire rope is proposed by theoretical analyses and also verified by finite element method (FEM) and experiments, which features much weaker magnetic interaction force and similar magnetization capability compared to the traditional yoke method. Meanwhile, the relevant detection apparatus or sensor is designed by simulation optimization. Furthermore, experimental comparisons between the new and yoke sensors for steel wire rope inspection are also conducted, which successfully confirm the characterization of smaller magnetic interaction force, less wear, and damage in contrast with traditional technologies. Finally, methods for SHM of steel wire rope and apparatus are discussed, which demonstrate the good practicability for SHM of steel wire rope under poor working conditions.

Keywords: steel wire rope, open magnetizer, structural health monitoring (SHM), notch filter, wavelet denoising

1. Introduction

Steel wire ropes are vital components concerning life safety and production, which usually operate in high-speed swaying conditions, therefore urgently being demanded to be monitored by nondestructive testing (NDT) methods for their structural health [1–8]. In most cases such as elevator, hoister in construction site, or in the mine, steel wire ropes are often driven by a friction wheel and run in turning motion with the aid of guide wheel, and then the dragging cages move up and down in a common working site. Owing to the spindle and soft features of

the ropes themselves (max length: 3000 m), high-speed (max: 15 m/s) swaying and nonuniform of loading, random shaking frequently happens to the operational ropes with a large distance (max: 50 mm) from detection sensors. What is more, due to poor service, various forms of steel wire rope failure such as corrosion, fracture, and fatigue wear frequently occur. Consequently, structural healthy monitoring (SHM) for steel wire rope plays a significant role in ensuring security and preserving assets.

As the detection apparatus or sensors, although some portable detection devices based on magnet yoke configuration have been developed, their magnetization and relevant detection depth are limited due to the limited permanent-magnet yoke configuration number and size. In view of these abovementioned, new SHM sensor and apparatus based on electric-magnetic flux leakage (MFL) detectors having adjustable and sufficient magnetizing strength by adjusting electric current compared to the permanent magnet-MFL ones for small radial steel rope [9] is proposed, which has powerful detection abilities, especially for the internal defects in steel wire ropes. More importantly, they are usually the first choice for high-speed MFL testing apparatuses for steel wire rope with large radius. Therefore, electromagnetic methods suitable for highly efficient SHM (fast detection) and antipollution are introduced.

Finally, owing to that steel wire ropes are composed of several strands of steel wires; another challenge of SHM for them is the signal classification or differentiating. Therefore, signal-processing methods are also discussed.

2. New SHM sensor and apparatus

2.1. SHM sensor and apparatus for the new proposed method

An electrical wire was discovered to generate magnetic fields by Hans Christain Oersted in 1820; as shown in **Figure 1(a)**, an electrical wire in a C-shape [10] will produce magnetic fields in the internal area of the arc. However, when applying electricity to the C-shaped wire shown in **Figure 1(b)**, the electrical current has both forward and backward directions. Accordingly, to further promote the magnetic-gathering actions of a carrying-current arc, we connect the arc to form a loop that is then formed into a C-shape configuration with an opening, as shown in **Figure 1(b)**. The magnetic fields at the arc center are theoretically very weak due to the offset of forward current (I) and backward current (I'), which can be calculated as follows:

$$B = B_1 - B_2 = \int_0^{\varphi} d(B_1 - B_2) = \int_0^{\varphi} dB_1 - \int_0^{\varphi} dB_2 = \left| \frac{\mu_0 I \varphi}{4\pi r_1} - \frac{\mu_0 I' \varphi}{4\pi r_2} \right|_{r_1 \to r_2} \to 0 \tag{1}$$

where μ_0 is the permeability of vacuum, φ is the angle of current element and radius vector, B_1 and B_2 represent the magnetic flux density produced by current I and I',r_1 and r_2 are the internal and external radii of the arc, respectively.

The magnetic fields inside the electrical arc are too weak to use for saturation magnetizing of the tested objects, which mainly arises from the offset of the "positive" and "negative" magnetic fields separately produced by the "forward" current (I) and "backward" current (I'), as shown in **Figure 1(c)** [11]. As a consequence, a ferrous core is arranged between the forward

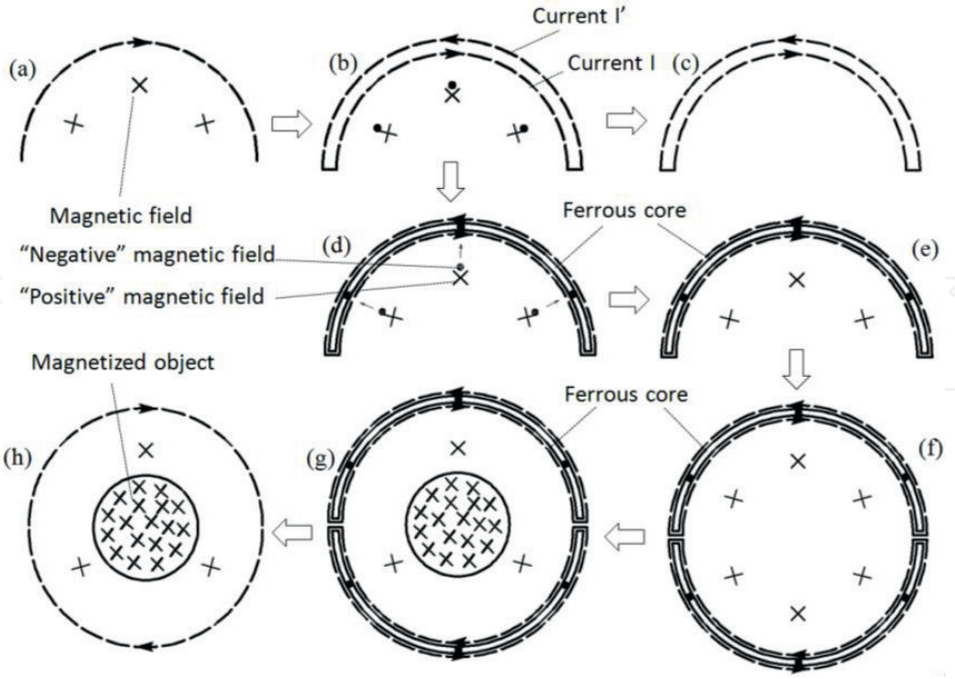

Figure 1. The magnetizing principle of an open coil. (a) Electrical wire in C-shape; (b) A loop with C shaped configuration; (c) Magnetic field inside the electrical arc; (d) Electrical wire in C-shape with a ferrous core; (e) Magnetic field inside the electrical arc with ferrous core; (f) Open coils with ferrous core; (g) Magnetic field produced by open coils in the magnetized object; (h) Magnetic field produced by conventional cylindrical solenoid in the magnetized object.

current (I) and the backward current (I'), as shown in **Figure 1(d)**; this core is designed to increase the "positive" magnetic fields (H) of the forward current using the magnetic-gathering effect. In addition, the ferrous core attracts the "negative" magnetic fields of the backward current (I') toward itself and removes this negative field from the arc center. By eliminating the negative effects caused by the backward current, the magnetic fields return to the value described in **Figure 1(a)**, as shown in **Figure 1(e)**. Finally, a magnetic field effect similar to the traditional electric annular loop can be obtained if the open coils are embedded with a ferrous core that consists of two identical half-open coils, as shown in **Figure 1(f)–(h)**. Finally, this configuration should produce a magnetic energy conversion region similar to a conventional cylindrical solenoid, as shown in **Figure 1(h)**.

Accordingly, a new open electric magnetizer is proposed, as shown in **Figure 2**, which consists of a C-shaped loop coil and a C-shaped ferrous core. This magnetizer primarily features an open mouth capable of encircling objects unlike the traditional tubular solenoid used as a magnetizer. Functionally, the proposed open magnetizer can center on an elongated object, such as in-service mine hoist wire ropes, to supply them with magnetization, which is beyond the capability of a conventional cylindrical electric magnetizer (i.e., solenoid). The advantage for elongated objects is illustrated in **Figure 2**.

The current electromagnetic methods failed to detect steel wire rope structures without heads and tails due to the tubular solenoids used as electro-magnetizers. Accordingly, a new SHM method based on the open magnetizer for steel wire rope without ends is proposed here. As schematically illustrated in **Figure 3**, the testing equipment consists of an open test probe, a direct current (DC) power supply, relevant data acquisition (DAQ) modules, and display

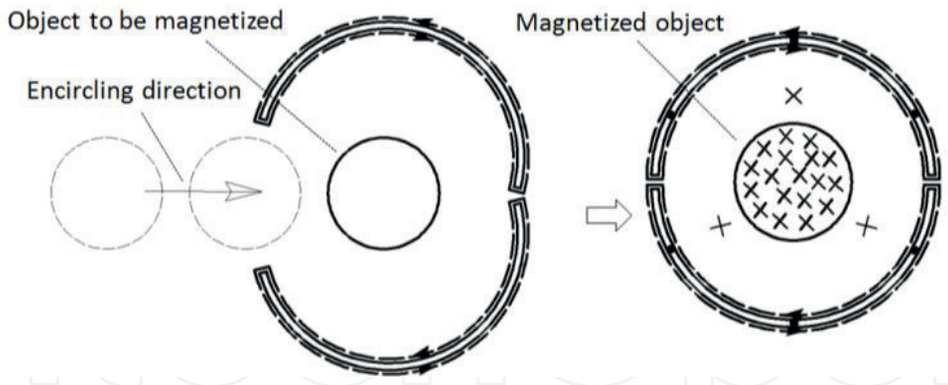

Figure 2. The proposed open electric magnetizer.

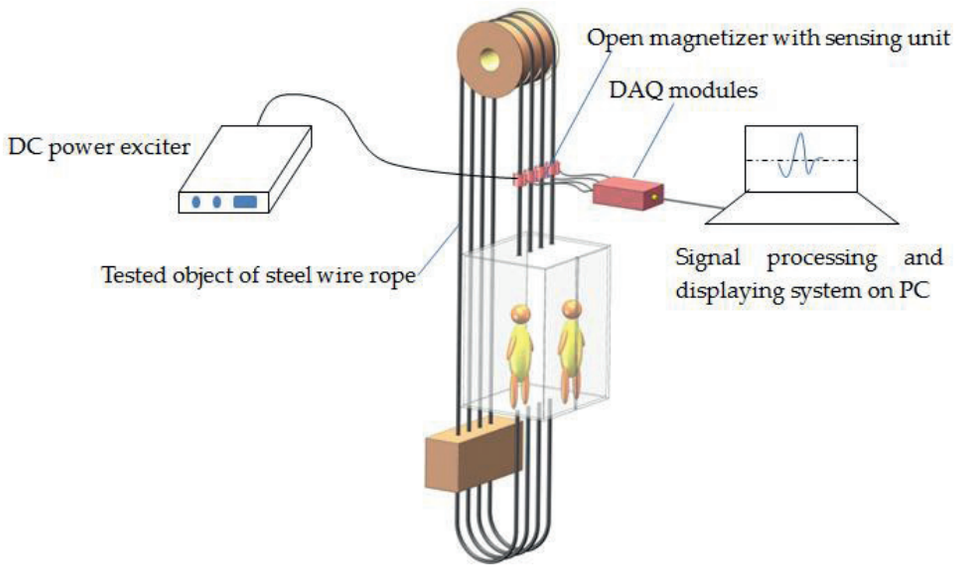

Figure 3. SHM methodology for steel wire rope using the open magnetizer.

software. The open test probe consists of an open magnetizer with magnetic-sensing units. The test procedure is as follows:

I. Encircle the steel wire rope in the center of the open magnetizer with a magnetic sensing unit. II. Apply DC power excitation to the open magnetizer coils and magnetize the steel wire rope. III. Scan the steel wire rope along the axial direction to acquire data and detect defects by moving the open magnetizer coils. IV. Observe and judge the signals from the displaying software on a personal computer (PC) to detect any defects.

An ANSYS simulation, as shown in **Figure 4(a)**, was built to describe a section of the open magnetizer and steel rebars; the internal diameter is 60 mm, the ferrous half C-shaped core is 15 mm thick, and the axial lengths of both the core and the coil are 120 mm. The tubular electromagnetic magnetizer consisting of the tubular coil has an internal diameter of 60 mm, a thickness of 15 mm in the radial direction, and an axial length of 120 mm, as displayed in **Figure 4(b)**. As indicated in **Figure 4(c)**, the specimen to be magnetized is a group of steel bars

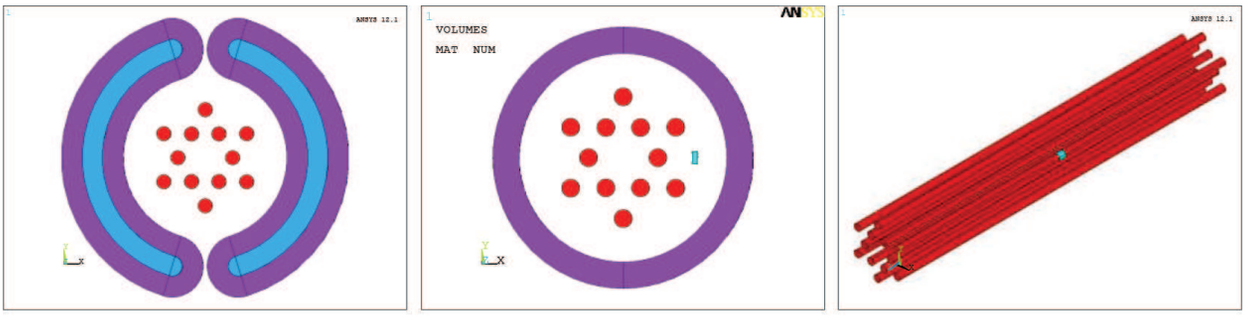

Figure 4. Three-dimensional models in the ANSYS simulations: (a) the sectional model of the open coil with the steel wire ropes; (b) the sectional model of the tubular coil with steel wire ropes; and (c) the model of the steel rope specimens with defects.

that have an axial length of 500 mm and a diameter of 10 mm; the axial distance between the outer steel wire rope and the magnetizer is 35 mm. Six steel wire ropes with defects in the axial direction were arranged in either the external layer or the internal layer at a 60° central angle. The Solid 117 element [12, 13] was chosen to build the three-dimensional models, and the magnetic permeability of the ferrous core was selected based on a B-H curve. Both sweep and free mesh methods [14, 15] were used to reduce the mesh number and to increase the symmetry of the mesh. For the mesh surrounding the defects in the steel ropes, the detailed mesh method was conducted to obtain more accurate calculations for the defect signals. The extracting operation was conducted in the route/path with an axial length of 120 mm and a diameter of 40.5 mm in the radial direction. The electrical current density was $J = 1e7\ A/m^2$ for both the open coil and the tubular coil. The open coil model was separated into four circular arcs that each have cylindrical coordinates to separately apply the electrical current density. The solution method was selected to be difference scalar potential, and the boundary condition is $Az = 0$. The extracting path for the signal is in the axial direction of the cylindrical coordinates, with a starting point of (41e−3, 0, −50e−3) and an ending point of (41e−3, 0, 50e−3).

Using the 3D models mentioned above, the magnetization function and effect, defect detection capability and magnetic force interaction of an open magnetizer coil and a tubular coil are compared. As shown in **Figure 5**, the whole magnetization status produced by the 3D models

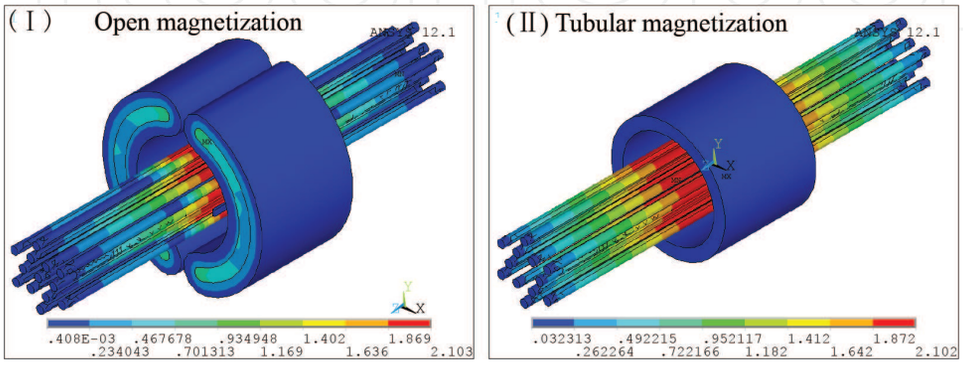

Figure 5. Magnetization status produced by the 3D models.

was obtained. The magnetic field density in both the radial and axial directions in the internal zone of the coils is displayed in **Figures 6** and **7**. As shown in **Figure 6**, the open magnetizer has a stronger radial magnetic field density, especially in the area close to the inner coils, than the tubular coils. **Figure 7** shows that the open magnetizer has a magnetization function and effect that is similar to that of the tubular one.

For the defect detection capability, the signals presenting the magnetic flux leakage density of both the internal and external defects in the steel wire ropes were obtained by path operation in the simulations, as shown in **Figure 8**. In this figure, "Open Inner" and "Open Outer" represent the signals excited by the open magnetizer coil, and "Traditional Inner" and "Traditional Outer" represent the signals excited by the traditional tubular magnetizer coil. Based on the simulation results shown in **Figure 8**, the open electromagnetic coil and the traditional tubular one have similar defect detection capabilities.

Figure 9 compares the magnetic force and shows that both the open magnetizer and the tubular one have approximate magnetic force interaction with the steel wire ropes. Therefore, these methods are suitable for defect detection, unlike permanent magnet magnetizers.

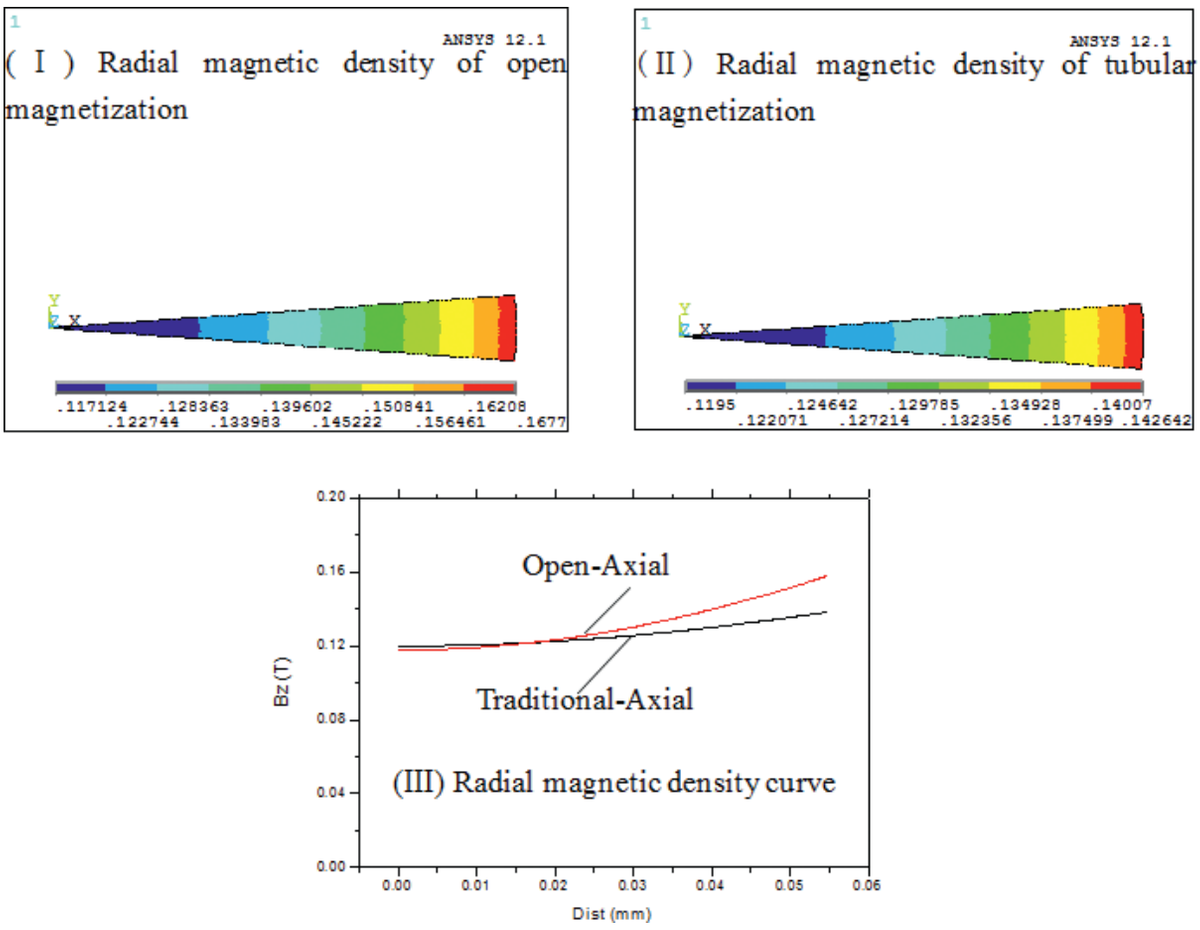

Figure 6. Magnetic field density in the radial direction inside the coils.

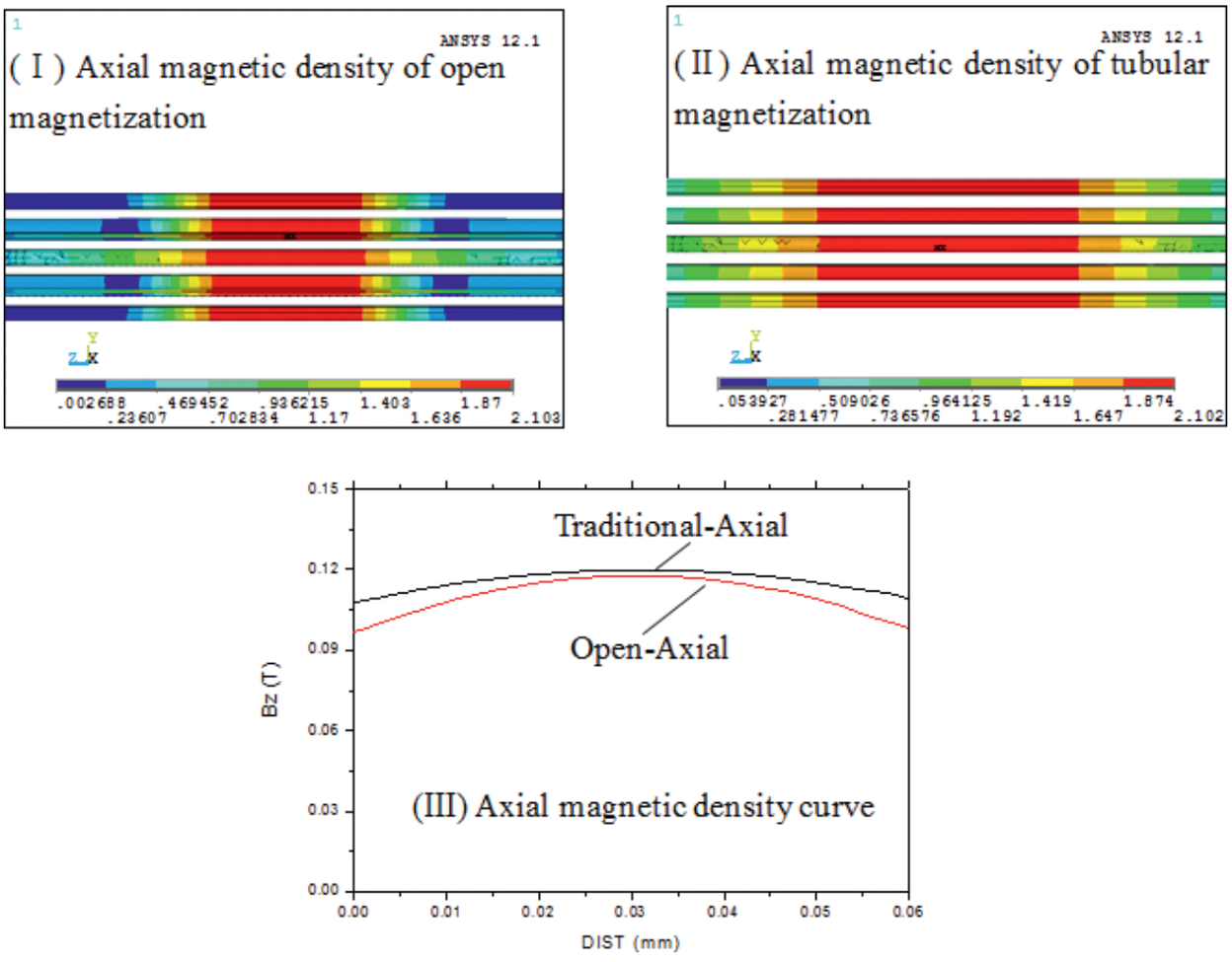

Figure 7. Magnetic field density in the axial direction inside the coils.

After finding similar magnetization effects and detect detection capabilities for both the proposed open electromagnetic coil and the traditional tubular one from the previous simulations, the open coil was further optimized. As shown in **Figure 10**, the relationships between the magnetization capability and the radial thickness, magnetic permeability and axial length of the C-shaped core were obtained. **Figures 10(a)–(c)** show that the optimum core is 15 mm in radial thickness, made of 45# steel and 120 mm in axial length.

Based on the previous analyses and optimization simulations, the traditional tubular coil and the open electromagnetic coil with a ferromagnetic core inside were designed and manufactured, as shown in **Figure 11**. The traditional tubular coil was mainly composed of copper wire wound outside the rubber mold. To verify the reliability and the validity of the simulations, optimized sizes for the magnetizer coils were chosen based on the analysis above. As illustrated in **Figures 11(a)** and **(c)**, the axial lengths of both magnetizer coils are 120 mm, the thickness of the open coil is 15 mm, and the material of the open electromagnetic core is 45# steel. The inner diameters of both magnetizer coils are 130 mm, based on the outer diameters of

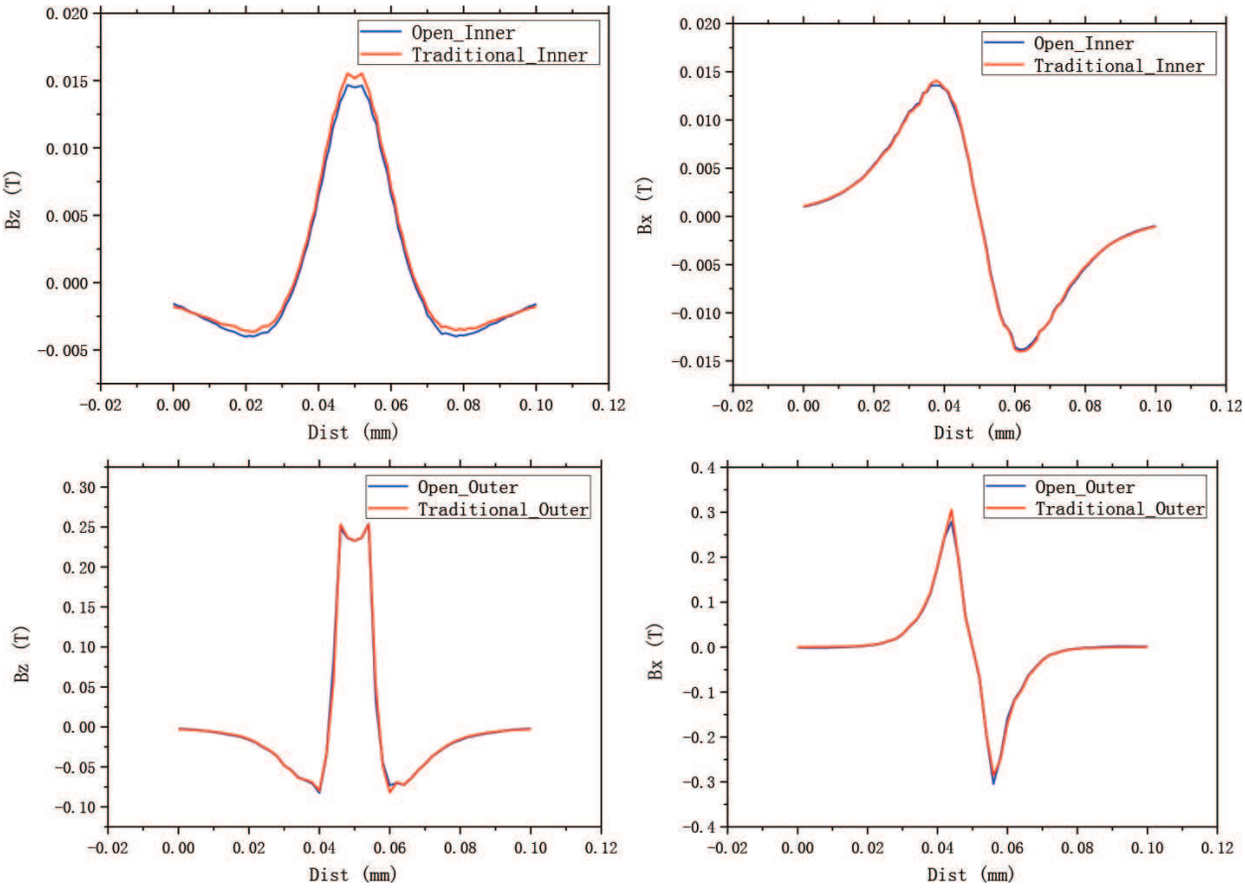

Figure 8. Comparison of the detection capabilities of the open and tubular magnetizers.

the tested concrete rebar, and are adjustable. Pictures of the actual electromagnetic coils are shown in **Figures 11(b)** and **(d)**.

First, a magnetization function experiment was conducted to measure the magnetic density using a Gauss meter, as shown in **Figure 12**. According to the simulations, both the radial and axial directions were tested, as shown in **Figure 12(a)**; **Figure 12(b)** shows the actual detection apparatus for these magnetizer coils.

These electromagnetic coils were magnetized using a DC source of 3A, and all of the magnetization data produced by the electromagnetic magnetizer were recorded by moving the magnetic sensor probe of the Gauss meter to different locations along the indicated radial and axial directions. The magnetic field densities in both the radial and axial directions inside the coils are displayed in **Figure 13(a)** and **(b)**; the coordinate "DIST" is the distance of the probe from the center of the coils. **Figure 13(a)** shows that the open magnetizer has stronger radial magnetic field density than the tubular coil, especially in the area close to the inner coil. As shown in **Figure 13(b)**, the open magnetizer has a similar magnetization function as the tubular one. All of the measurement results are in accordance with the simulation results.

Furthermore, an experimental apparatus simulating detection was built. After the experiments were conducted, the detection signals for the man-made defects were saved, as shown in **Figure 12**. Using different directions of the hall element sensor inside the magnetizing coils,

http://dx.doi.org/10.5772/intechopen.68148

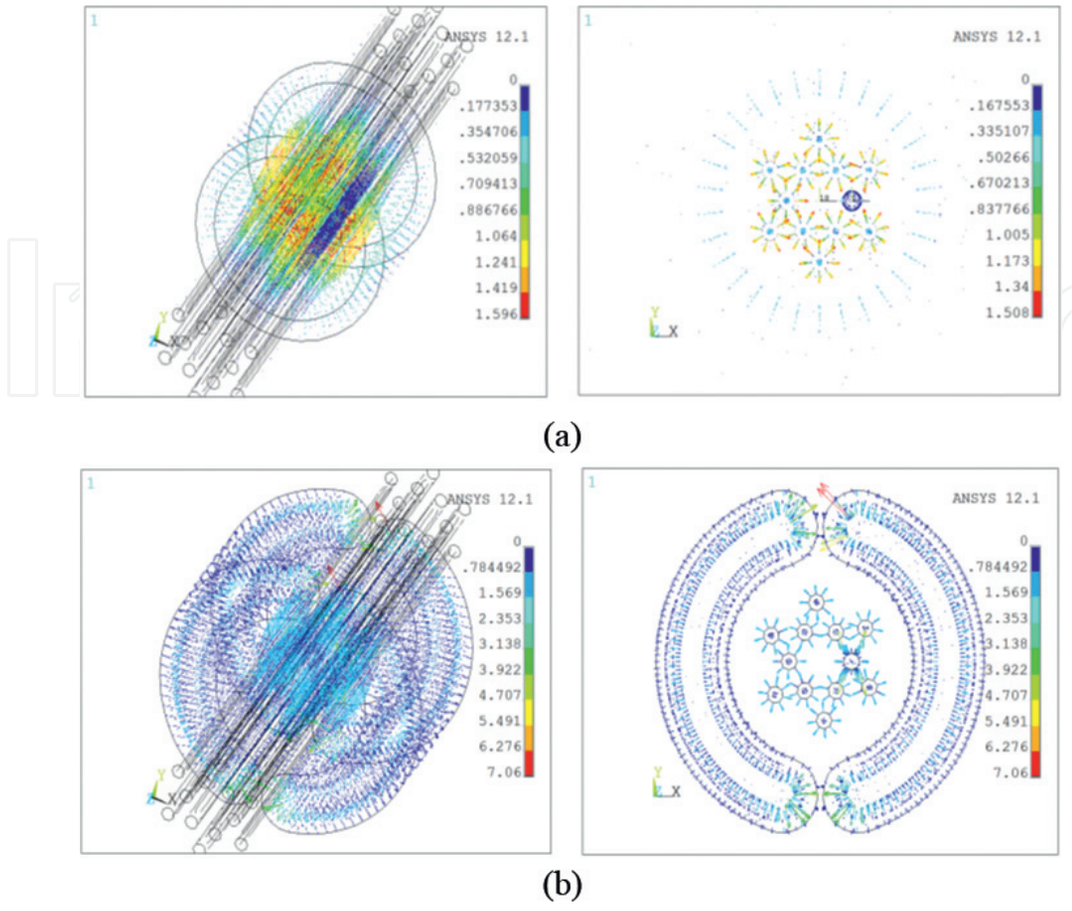

Figure 9. Comparison of magnetic force of tubular and open magnetizers. Magnetic force interaction of (a) tubular coils and (b) open coils.

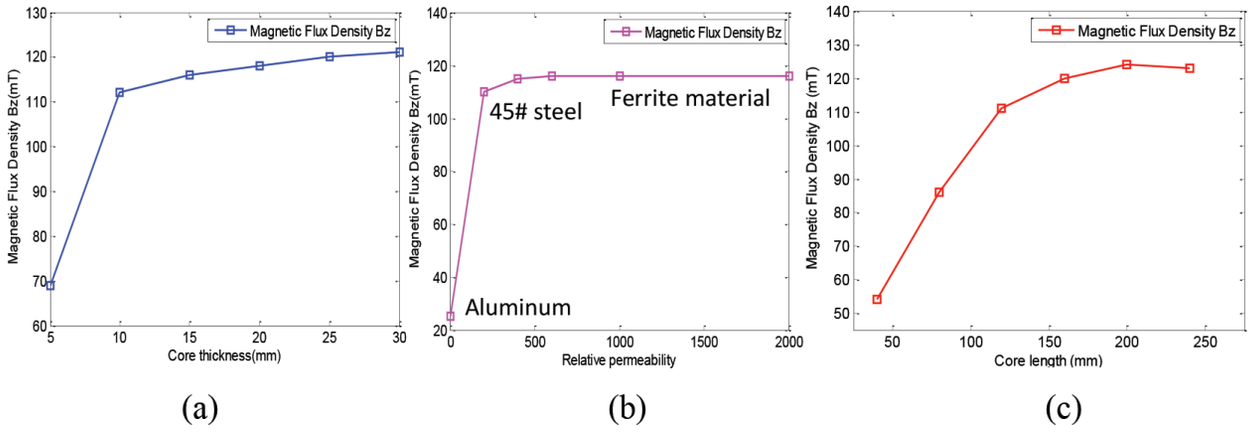

Figure 10. Relationships between the magnetization capability and the structural parameters of the core: (a) relationship between the magnetization capability and the radial thickness of the core; (b) relationship between the magnetization capability and the magnetic permeability of the core; and (c) relationship between the magnetization capability and the axial length of the core.

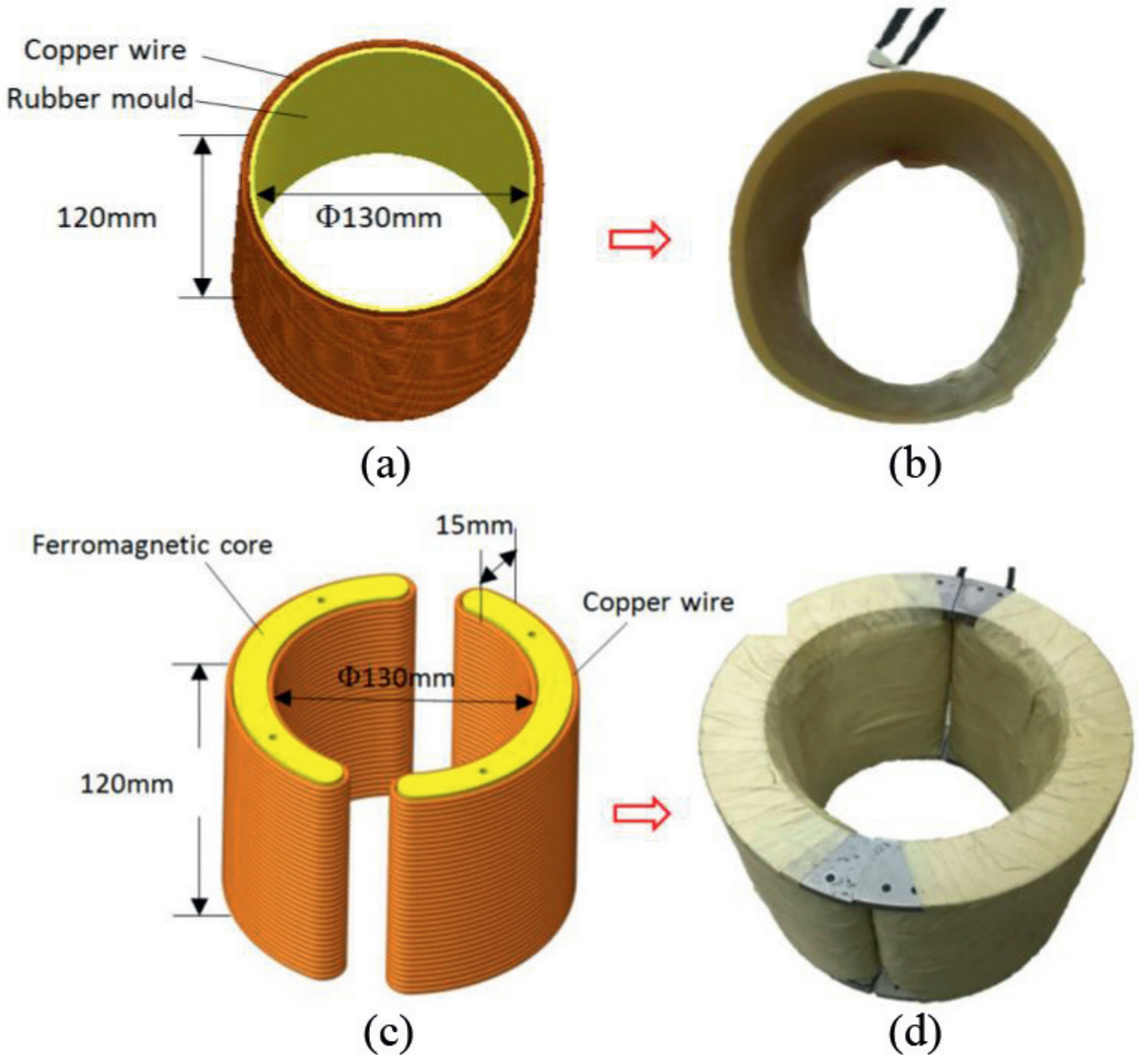

Figure 11. Traditional tubular coil and the proposed open electromagnetic coil. (a) Schematic diagram of the tubular coil; (b) actual tubular coil; (c) schematic diagram of the open coil and (d) actual open electromagnetic coil.

the axial and radial amplitudes of the MFL signals were obtained. The used 3551-Hall-array sensor is located closely to the internal wall of the open coil at the center of the coil in its axial direction. The moving speed of the detection probe for scanning is about 0.25 m/s with respect to the concrete rebar.

According to the signals shown in **Figure 14**, "Traditional" represents signals that were acquired by the traditional magnetizing tubular coil, as mentioned in **Figure 11(b)**, while "Open" means that the signals were obtained using the novel open electromagnetic coil, as described in **Figure 11(d)**. Similarly, "Inner" and "Outer" denote that the signals were produced by defects in the internal layer and the external layer, respectively.

As shown in **Figure 14(a)** and **(c)**, both magnetizing coils have a strong ability to detect internal defects; in addition, the defect signals from the external layer are stronger than those of the

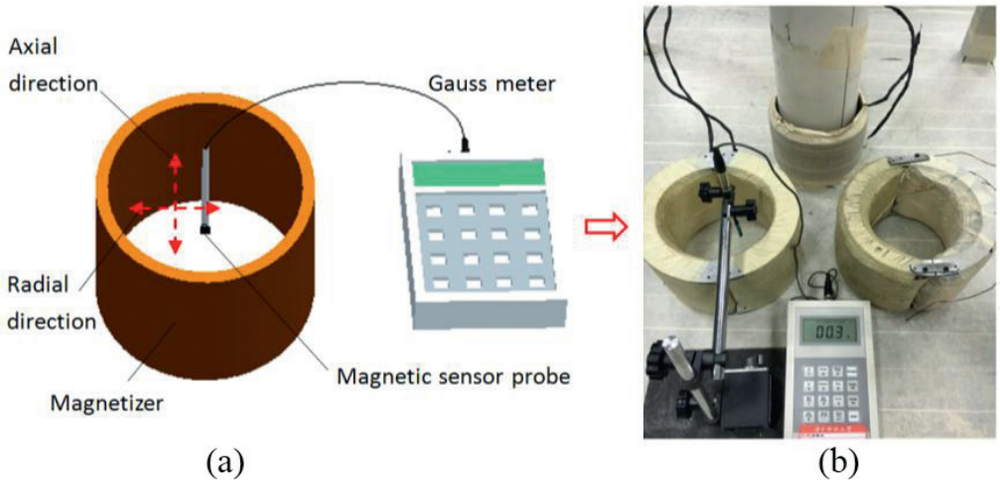

Figure 12. Magnetic density detection experiment. (a) Magnetic density detection using a Gauss meter and (b) actual detection apparatus.

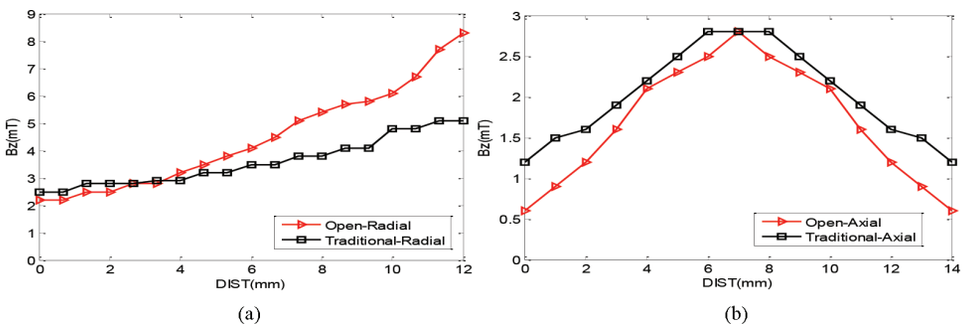

Figure 13. Magnetic density measured using the Gauss meter. (a) Radial magnetic density of the open and traditional coils measured using the Gauss meter and (b) axial magnetic density of the open and traditional coils measured using the Gauss meter.

internal layer. Moreover, the signals excited by the open electromagnetic coils are very similar to those of the traditional tubular coils. Furthermore, the experimental results are consistent with the simulation results shown in **Figure 8**, demonstrating the validity of the open electromagnetic technique proposed in this chapter.

2.2. Comparison of magnetic open and yoke MFL testing method

To address the hoist wire rope inspection challenges, this chapter also presents an open magnetization sensor possessing the advantages over yoke magnetization method [16–20] in terms of magnetic excitation capability and magnetic interaction force. Furthermore, this chapter also intends to design a relevant detection sensor based on open permanent magnetization method by optimization and a testing probe configuration capable of tracking swing rope by experimental comparison of MFL signal change trends. Finally, the chapter developed a corresponding portable testing apparatus with great promise of application performance in the future.

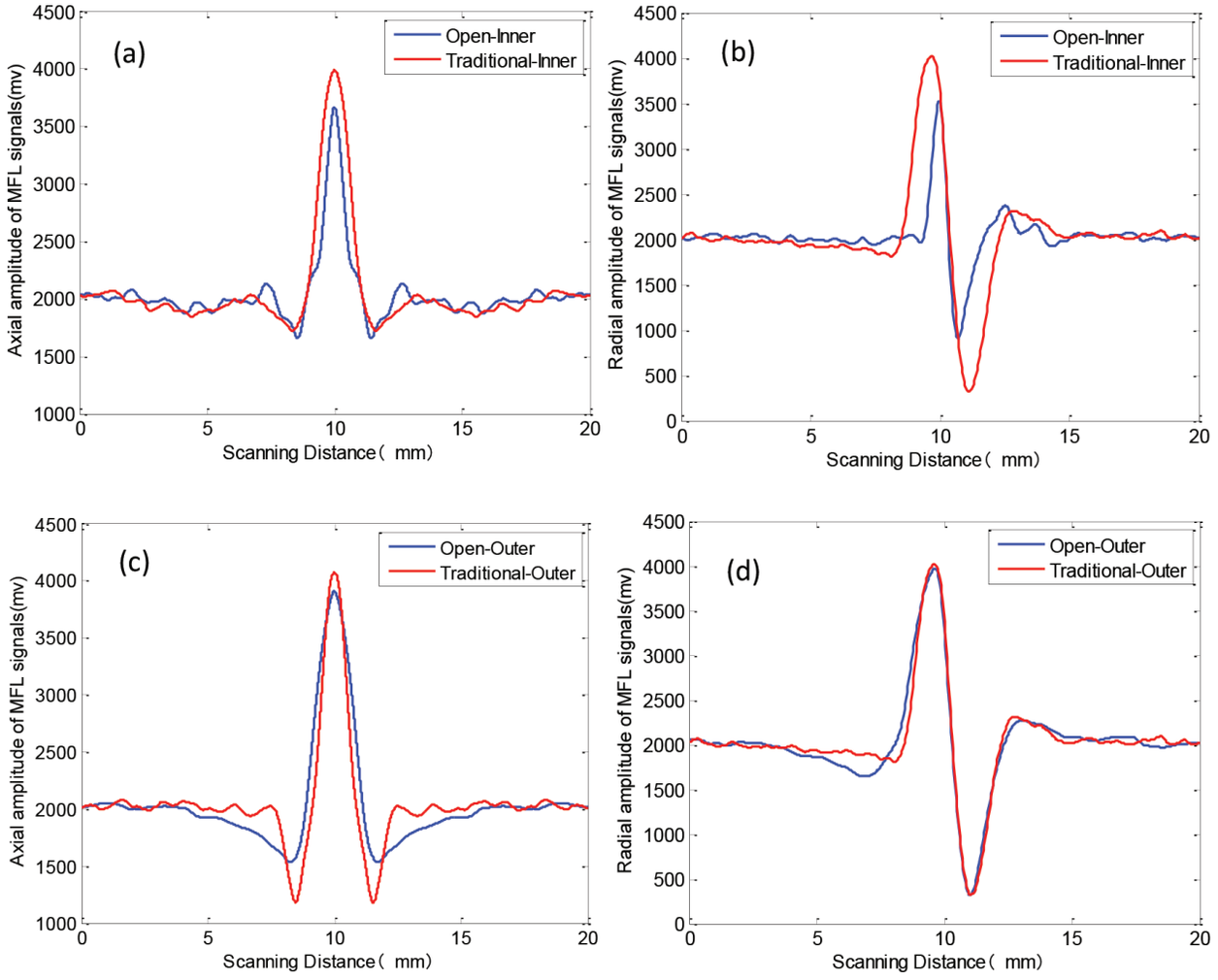

Figure 14. Experimental results of the defect detection capability of the two magnetizer coils; (a) Axial MFL signals by open and traditional coils for inner layer defects detection; (b) Radial MFL signals by open and traditional coils for inner layer defects detection; (c) Axial MFL signals by open and traditional coils for outer layer defects detection; (d) Radial MFL signals by open and traditional coils for outer layer defects detection.

Presently, the commonly used portable MFL testing instrument for static wire rope defect detection mainly consists of several magnetic-yoke testing packages. Each of them is composed of double permanent magnets stacks with magnetic poles facing closed to the tested object, ferrous yoke connecting the stacks, and magnetic-sensing units fixed under the yoke and adjacent to the poles. The magnetic-yoke MFL testing method for wire rope is schematically illustrated in **Figure 15**. To magnetically saturate the object being detected, the double magnetic poles should be located closely to the tested wire rope as much as possible, together with the sensing units, leading to a small lift-off distance (1–5 mm) for each package relative to the tested wire rope. Additionally, the ferrous yoke also should be designed at a certain length (over 240 mm) and height (over 50 mm) to ensure a linear working range for some magnetic sensors such as hall element. In consideration of these above, the current yoke-type MFL testing sensor is characterized by strong magnetic force interaction (at least 300 N) with the ropes, large volume (at least 240 mm in length), large weight (at least 9 kg in weight), and poor adaptability for tested wire ropes with different diameters. Consequently, with respect to the

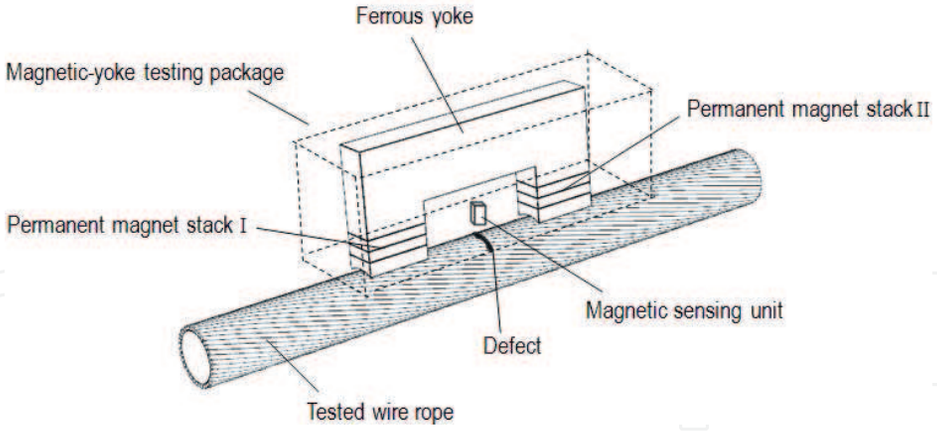

Figure 15. Testing principles based on yoke-magnetizing method for wire rope.

portable mine hoist wire ropes running in a high-speed-swaying status, the existing magnetic-yoke method is hard to perform the task of hoist wire rope detection.

Differing from the magnetic circuit principles mentioned above, an open magnetization method hopefully created by a ring-shaped magnet is here provided in contrast with the commonly used ring-shaped coils, which apply open magnetization technique to magnetize the detected objects. According to magnetic charge and molecular flow theory, the description for the magnetic potential ϕ_m at an arbitrary point of P outside the permanent is

$$\phi_m = \frac{1}{4\pi}\oint_S \frac{M \cdot n}{R} dS + \frac{1}{4\pi}\oint_\tau \frac{\nabla \cdot M}{R} d\tau \tag{2}$$

where M is the magnetic strength of permanent magnet, S is the curved surface encircling the magnet, R is the distance between the source point to the field point, n is normal to the external surface of magnet, and ∇ is divergence operator.

Owing to the uniform magnetization, the ring-shaped magnet manifests itself by surface current and features no body current. Therefore, there is equivalent electric current density for area of $\rho_{\mathrm{sm}} = M \cdot n$ and for volume of $\rho_m = \nabla \cdot M = 0$.

Thus, Eq. (2) can be

$$\phi_m = \frac{1}{4\pi}\oint_S \frac{\rho_{sm}}{R} dS \tag{3}$$

Then, combined with Obi-Wan thrall's law (i.e., $H = -\nabla \cdot \varphi_m$), magnetic flux density can be obtained by

$$H = \oint_S \frac{\rho_{\mathrm{sm}}}{4\pi} \cdot \frac{R}{R^3} dS \tag{4}$$

As shown in **Figure 16(a)**, the magnetic field density produced at an arbitrary point $P(\rho, \varphi, \mathrm{h})$ can be further calculated as

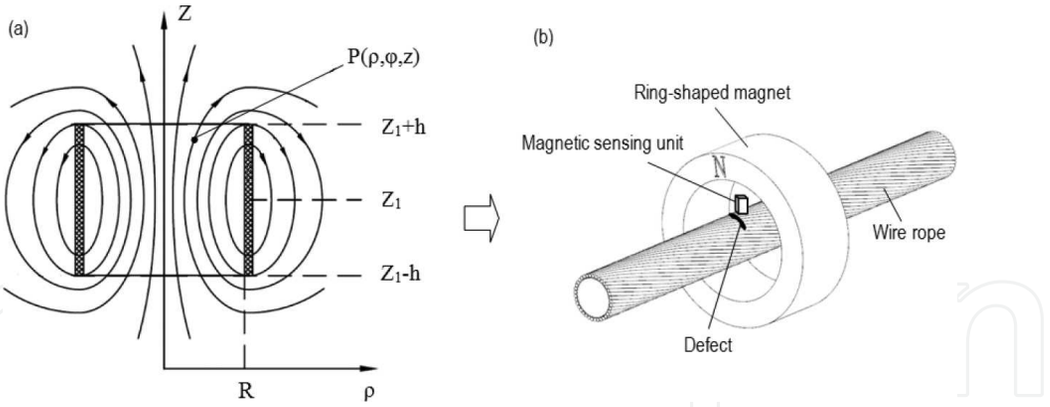

Figure 16. Testing principles based on open-magnetizing method; (a) Magnetic field density produced at an arbitrary point by the coil; (b) Ring shaped magnetizer in wire rope detection.

$$H(\rho,\varphi,h)=\frac{M}{4\pi}\iint_{S_+}\frac{(\rho-x)i+yj+(h-z)k}{\left((\rho-x)^2+y^2+(h-z)^2\right)^{3/2}}dS-\frac{M}{4\pi}\iint_{S_-}\frac{(\rho-x)i+yj+(h-z)k}{\left((\rho-x)^2+y^2+(h-z)^2\right)^{3/2}}dS \quad (5)$$

Furthermore, the magnetic field strength produced by the ring-shaped magnet can be obtained by vector sum, described as

$$H(\rho,\varphi,h)_{R-r}=H(\rho_R,\varphi,h)-H(\rho_r,\varphi,h) \quad (6)$$

Finally, the magnetic flux density in the magnetized body (relative magnetic permeability μ) provided by the open magnetization method can be obtained as

$$B(\rho,\varphi,h)=\mu\cdot H(\rho,\varphi,h) \quad (7)$$

Unlike the abovementioned conventional magnetic-yoke method, learning from the widespread solenoid coil as a magnetizer in fixed MFL apparatuses, a new ring-shaped MFL testing method is proposed here, as displayed in **Figure 16**. Here, a ring-shaped permanent magnet is adopted to axially magnetize the whole circumference of the tested wire rope at a certain length similar to a tubular solenoid coil does, and unattached magnetic-sensing units covering the full circumference of the tested rope are separately placed inside the ring magnet, as indicated in **Figure 16(a)**. Owing to the ring-shaped open magnetization configuration, the magnetic interactions between the magnetizer and wire rope are largely decreased. On account of that, the full circumference magnetizer is like a tubular coil with excitation current, as shown in **Figure 16(b)**; the ring-shaped magnetizer can be designed with a larger space inside for separately disposing the magnetic-sensing units with various sizes correspondingly to different wire ropes. As a consequence, the provided method owns the advantages of small magnetic force interactions with the tested ropes, simple configuration for realization, and all-purpose magnetizer characteristics for various-sized wire ropes.

2.3. Simulation results

Finite element method (FEM) was applied to simulate and analyze the comparisons, and the two above-presented magnetization methods were modeled for a same steel wire rope (rope

diameter of 32 mm and length 300 mm, dextral rope strand number of 19) with a broken wire (defect diameter of 1.2 mm). The two models consist of a ring-shaped permanent magnet (axial length 80 mm, internal diameter 70 mm, and external diameter 100 mm) as an open magnetizer and six magnet yokes (yoke width 24 mm, yoke height 20 mm, yoke length 180, leg length 10 mm, leg spacing 100 mm, and yoke lift-off 8 mm) as a yoke magnetizer, respectively. In the former model, to ensure the versatility of an open magnetizer for different sized wire ropes, radial spacing should be somewhat larger and the size of 20 mm is selected here. By experience in practice application, a certain length (60 mm) of the middle of the ring-shaped magnet is replaced by a ferrous ring-shaped configuration with the same size either for the installation convenience of magnetic-sensing units or reducing cost. During the course of the simulations, the coercive force and relative magnetic permeability of permanent magnets made of NdFeB material were, respectively, 490,000 A/M and 1, and all the ferrous materials had the magnetic permeability based on a B-H curve. Finite element was chosen by Solid 236 and 3D 20-node element, which is applicable to 3D static electromagnetic analyses and to modeling air, iron, nonferrous materials, and permanent magnets. Additionally, the Solid 236 can be used with command macros such as "EMAGERR (electromagnetic relative error)" for calculating relative error and "EMFT (electromagnetic forces and torques)" for summarizing electromagnetic forces. Two finite element models were obtained by the usage of sweep mesh combined with free mesh for both high resolution and fast computation, as presented in **Figure 17(a)** and **(b)**, respectively.

After solving the finite element models designed above, magnetization results for the steel wire ropes were obtained, as displayed in **Figure 18**. In **Figure 18(a)** and **(b)**, it can be observed that both of the methods produce the similar magnetic flux density at the magnetizing center of the wire ropes and they are capable of carrying out similar magnetically saturated statuses for the objects. Therefore, we can draw a conclusion that the performance of the magnetic excitation provided by the open magnetization method for detecting defects is similar to that supplied by the traditional yoke one.

MFL sensors accomplish their defect scanning for the tested objects by dynamic contact and sliding friction. Magnetic interaction force between MFL sensors and tested objects has a great influence on the service life of both sensors and tested objects due to wear or impact damage. Additionally, great magnetic interaction force also affects the steady location in the center of the

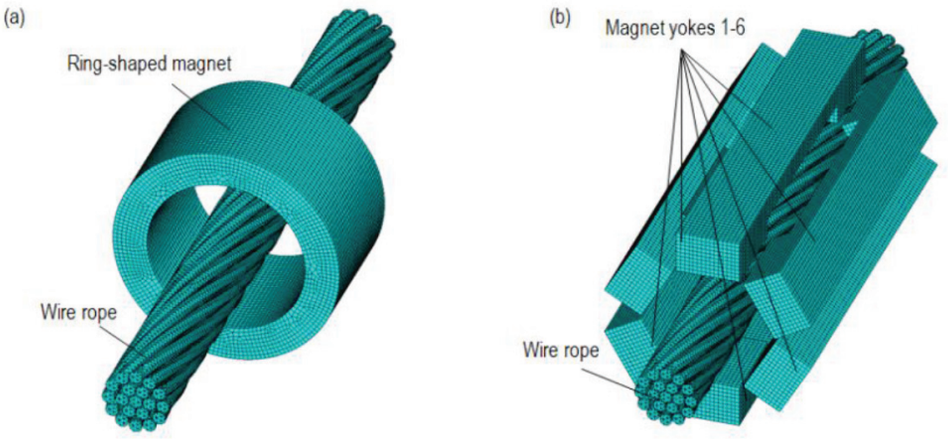

Figure 17. FEM models for open and yoke method; (a) FEM models for open method; (b) FEM models for yoke method.

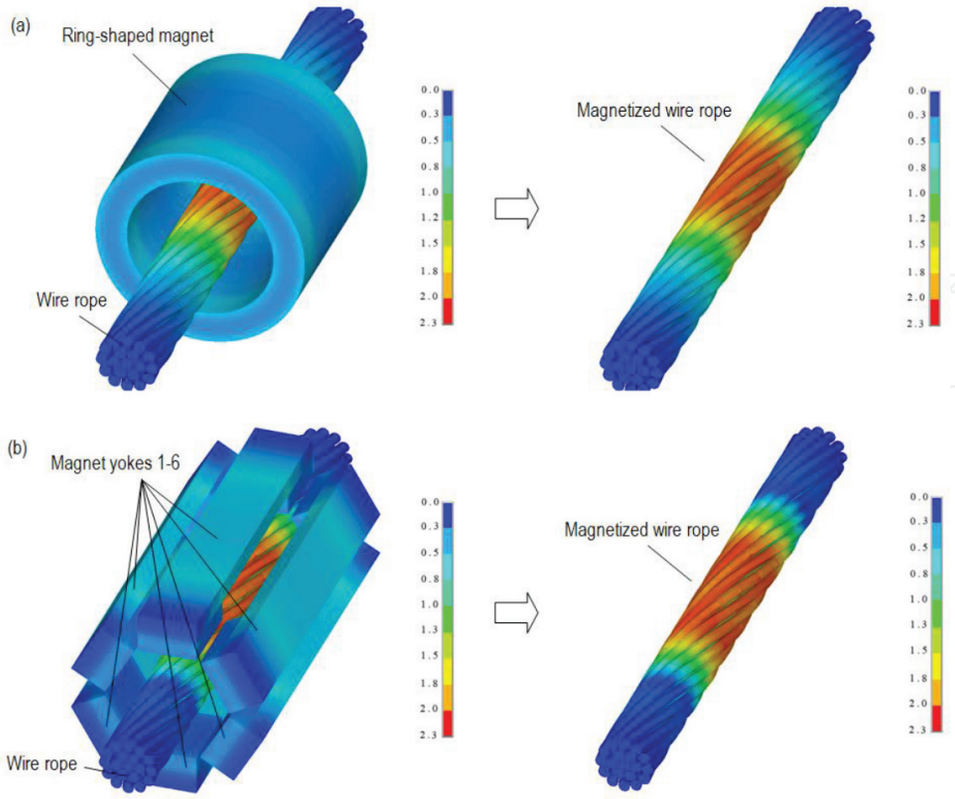

Figure 18. Magnetization capabilities for wire ropes, respectively, provided by open and yoke method; (a) Magnetization capabilities for wire ropes by open method; (b) Magnetization capabilities for wire ropes by yoke method.

magnetizer and the quick realization for detaching the sensor from the tested object. These problems are apparent in the portable inspections for the elongated objects in service. Therefore, the magnetic interaction force brought out by relevant methods should be concerned. Considering that MFL sensors are usually designed into two half parts to encircle the tested objects, the magnetic interaction force generated by the double half structures of both magnetization methods was extracted by vector plot of FMAG (magnetic force), as shown in **Figure 19**.

Furthermore, the detailed values of magnetic forces were calculated and summarized by directly using the command stream of FEM tool ANSYS of "EMFT," and the forces were stored as items F_x, F_y, F_z, and F_{total} parameters, as shown in **Table 1**.

The items of F_x, F_y, and F_z are the magnetic force component in Cartesian coordinate system listed in **Table 1**, and F_{total} is the vector sum magnetic force of these components.

Figure 19 and **Table 1** demonstrate that the magnetic interaction force produced by the yoke magnetization method is seven times stronger than that caused by the open one especially for the component of F_y and F_{total}. Hence, a conclusion can be drawn that the open magnetization method can realize detaching the sensor from the tested object more easily and meanwhile causes less wear and damage to them compared with the yoke one. Consequently, the open magnetization method is more suitable for portable detections of hoist wire rope and owns a much longer service life. The detailed distributions of the magnetic interaction forces to the wire ropes caused by the both magnetizers can be seen in **Table 2**, respectively.

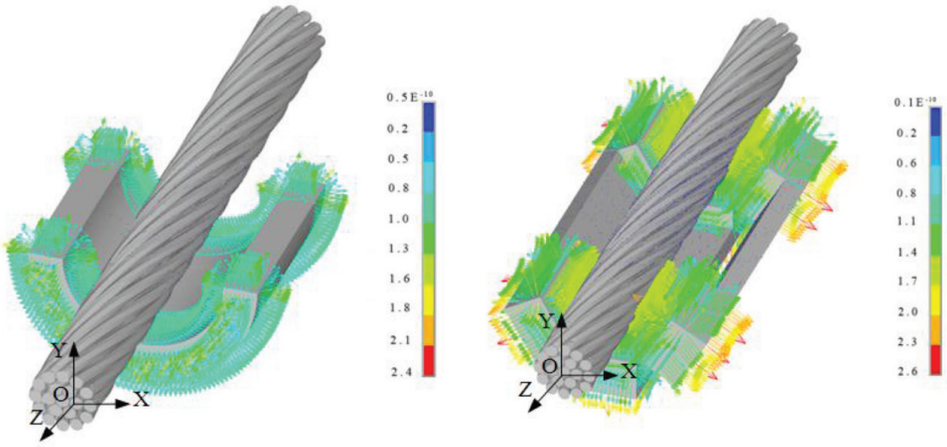

Figure 19. Magnetic interaction forces, respectively, caused by open and yoke model.

Model types	**Force types (N)**			
	F_x	F_y	F_z	F_{total}
Open method	0.01	45.30	0.0	45.30
Yoke method	0.02	360.01	0.0	360.01

Table 1. The summary results of the magnetic interaction force.

Model types	**Force types (N)**			
	F_x	F_y	F_z	F_{total}
Open method		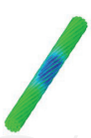		
Yoke method		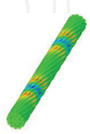		

Table 2. The detailed distributions of the magnetic interaction forces simulated by open and yoke method.

Regarding the primary design of open magnetization MFL sensor mentioned above, much attention should be focused on the ring-shaped permanent magnet magnetizer. Similar to the ring-shaped coil, the basic sizes of the ring-shaped permanent magnet sensors are axial length and the radial thickness. During the simulations, to maintain enough assembly space for the magnetic-sensing units, the distance between the surface of the tested wire ropes and the inner center of ring-shaped magnet always remained at 20 mm. The picking-up route of the

magnetic field value (axial component of B_y and radial component of B_z) was set to be 20 mm in axial length and 1 mm in radial lift-off. Thereafter by changing relevant sizes of permanent magnet and picking up the magnetic fields via the specified route, the MFL signal waveforms produced by the broken defects of wire ropes were obtained as well as the curve of their peak-to-peak value, as demonstrated in **Figure 20**.

Similar to the commonly used tubular coils, the conclusion drawn from **Figure 20(a)** and **(b)** is that the larger axial length and radial thickness sizes that the ring-shaped magnet have, the stronger MFL signals would produce from wire rope defects when the axial length and radial thickness of the ring-shaped magnet are, respectively, less than 300 and 70 mm. Combed with the requirements of low cost in practice application as described previously, the middle part of the whole ring-shaped permanent magnet is creatively replaced by a ring-shaped ferromagnetic material while the two sides of the ferrous ring remain magnets. Therefore, **Figure 20(c)** and **(d)** were gained, which indicated that the MFL signals decrease with the increasing axial length of the ferromagnetic ring with a turning point of 80 mm and the MFL signal is the strongest when radial thickness of the ferromagnetic ring is 15 mm. Actually, permanent magnet ring was just defined by 15 mm according to practice experience at that time. Indeed, it has also been confirmed that the MFL is the strongest when the radial thickness of the ferromagnetic ring is the same as the permanent ring by additional simulations. As a result and combined with practice engineering application, the ferromagnetic ring is designed to be 80 mm in axial length and 15 mm in radial thickness, and the inner diameter is at least 70 mm to meet the testing requirement for various detected objects with different sizes.

2.4. Experimental results of the defect detection

Based on the simulation and size optimization done above, the open magnetization MFL sensor for wire ropes is designed, as displayed in **Figure 21**, which is simply composed of two parts, namely a ring-shaped magnet and its unattached ring-shaped shoe including magnetic-sensing units. The size specifications of ring-shaped shoes can be immediately obtained by changing its internal diameters, and one ring-shaped sensor can easily accomplish all the detections for different sized objects just through replacing the relevant size specifications of ring shoes. Explanatorily, the middle length of the ring magnet in its axial orientation is designed to be replaced by a ferromagnetic ring so that the unattached ring-shaped shoes could easily be fixed inside the inner ring and the whole cost could be reduced. Owing to that, the hoist wire ropes are fixed by carrying cages at both sides and have no head and tail, the designed open magnetizing sensor is easily designed into two-half structure in practice, which merely has the configuration sizes of 120 mm (length) $\times$ 100 mm (diameter) and just weighs about 1.5 kg, featuring small volume and weight.

As indicated in **Figure 22**, the open magnetization MFL sensor designed above was tested for the detection capability of a man-made broken-wire defect in a wire rope (Φ32 mm) and the magnetic force interaction with the tested wire rope. During the course of experimental testing for detection capability, the sensor was connected with an amplifier, a filter, an A/D converter, and a data analysis system in serials. By linear axial scanning along the rope, the output signals from the artificial broken wire were finally acquired, demonstrating that the proposed MFL

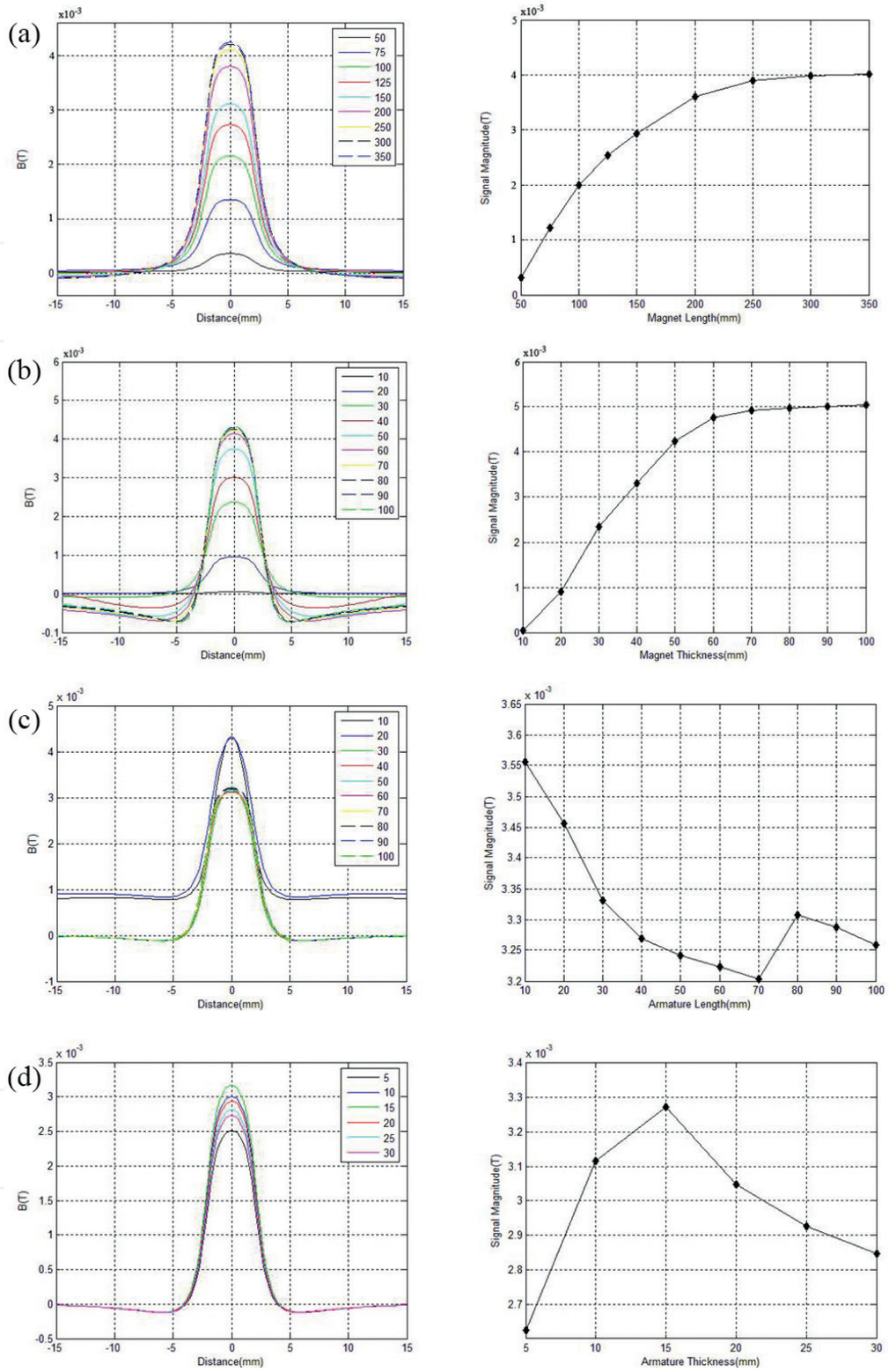

Figure 20. The MFL signals of a broken-wire defect with the changing of ring-shaped open magnetization MFL sensor sizes. (a) The MFL signals of a broken-wire defect with the changing of axial length of ring-shaped magnet. (b) The MFL signals of a broken-wire defect with the changing of radial thickness of ring-shaped magnet. (c) The MFL signals of a broken-wire defect with the changing of axial length of the ferromagnetic ring between two magnet rings. (d) The MFL signals of a broken-wire defect with the changing of radial thickness of the ferromagnetic ring between two magnet rings.

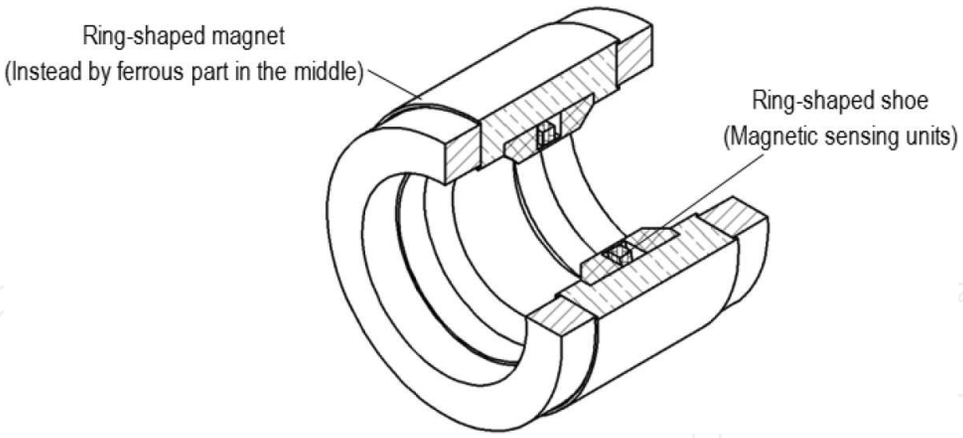

Figure 21. Open magnetization MFL sensor for steel wire rope testing.

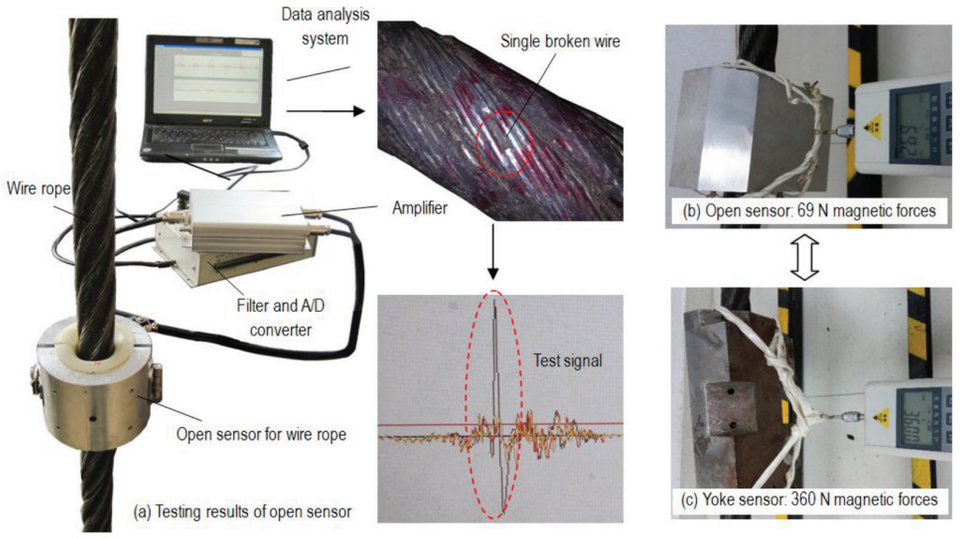

Figure 22. Experimental results of the defect detection capability and magnetic interaction forces.

sensor owns the inspection capability even for a single broken wire as the traditional yoke sensor does. Most notably, the testing for the magnetic interaction force produced by the created open sensor is only 69.2 N, while that caused by the traditional yoke one is over 360 N, which demonstrates that the new proposed open magnetization sensor features a much weaker magnetic interaction force compared with the yoke sensor and accords with the theoretically FEM analyses done before.

3. Conclusion

The life expectancy of a hoist structure largely depends on the properties of the steel wire ropes; many studies on the nondestructive evaluation of concrete are being developed.

However, many existing methodologies and techniques fail to detect steel wire rope defects, especially in sophisticated circumstances. Using tubular coils, the MFL technique has developed rapidly. However, the closed structure limits the detection scope of traditional tubular coils and prevents the testing of very long objects, such as stay cables. Moreover, a large number of studies regarding SHM focus on the electromagnetic technique, while very little literature has reported on their validity for steel wire rope detection. In short, the current electric-MFL SHM methods using tubular coils as the electro-magnetizers fail to detect steel wire ropes without a head and a tail.

Therefore, a novel electric-MFL SHM technique for concrete rebar using open electromagnetic coils as the magnetizers is presented; this open configuration is preferable for the defect detection of closed or very long structures of tested objects and has wider applications in the SHM of steel wire ropes. Based on the traditional tubular coils, a novel electromagnetic testing apparatus with an open magnetizer is proposed for theoretical analysis and comparison. Next, finite element modeling and simulation based on ANSYS are conducted, and the magnetization effect, defect detection capability, and magnetic force interaction are studied and compared. Furthermore, an optimized magnetizer structure is also presented.

To validate the reliability and validity of the simulations, two optimized magnetizers are designed and manufactured; then, experiments are conducted to determine the magnetization effect and the defect detection capability of the two magnetizing coils. The experimental results showed that the proposed open electromagnetic technique has a similar magnetization effect and an excellent defect detection capability compared to the traditional tubular coils. Finally, the consistency between the simulation and experimental results confirmed the great potential of concrete SHM using the open electromagnetic technique.

Additionally, a new sensor based on open magnetization method is characterized by weaker magnetic interaction force, and similar magnetization capability compared to the traditional yoke method is also proposed. Therefore, the novel testing sensor of the MFL testing method with these advantages is more suitable for portable defect detections of hoist wire ropes, featuring good signal-to-noise rate by reducing magnetic noises produced by rope swaying, little wear or damage and full automatic detection process. Meanwhile, the new testing sensor with preponderant characteristics further promotes the capability of addressing the challenges of portable hoist wire ropes to maintain a constant lift-off distance for scanning. The final practice applications confirm the availability and validity of the portable MFL testing apparatus for the nondestructive testing of hoist ropes under poor working conditions.

Acknowledgements

This chapter was financially supported by the National Natural Science Foundation of China (51475194), the National Key Basic Research Program of China (2014CB046706), and the Fundamental Research Funds for the Central Universities (Grant No. 2015MS015).

Author details

Shiwei Liu, Yanhua Sun* and Wenjia Ma

*Address all correspondence to: yhsun@hust.edu.cn

School of Mechanical Science and Engineering, Huazhong University of Science and Technology, Wuhan, China

References

[1] Mehrabi AB. In-service evaluation of cable-stayed bridges, overview of available methods and findings. Journal of Bridge Engineering. 2006;**11**(6):716–724

[2] Xu F, Wang X, Wu H. Inspection method of cable-stayed bridge using magnetic flux leakage detection: Principle, sensor design, and signal processing. Journal of Mechanical Science and Technology. 2012;**26**(3):661–669

[3] Jomdecha C, Prateepasen A. Design of modified electromagnetic main-flux for steel wire rope inspection. Ndt & E International. 2009;**42**(1):77–83

[4] Kwun H, Cecil MTII. Nondestructive evaluation of ferromagnetic cables and ropes using magnetostrictively induced acoustic/ultrasonic waves and magnetostrictively detected acoustic emissions: U.S. Patent 5,456,113; 1995

[5] Makar J, Desnoyers R. Magnetic field techniques for the inspection of steel under concrete cover. NDT & E International. 2001;**34**(7):445–456

[6] Zhong XY, Zhang XH. Research of on-line detection apparatus for industrial steel wire rope. Applied Mechanics and Materials. Trans Tech Publications. 2011;**48**:924–927

[7] Zawada K. Magnetic NDT of steel wire ropes. Journal of Nondestructive Testing & Ultrasonics (Germany). 1999:4(8):1–1

[8] Wait JR. Review of electromagnetic methods in nondestructive testing of wire ropes. Proceedings of the IEEE. 1979;**67**(6):892–903

[9] Sun Y, Liu S, Li R, et al. A new magnetic flux leakage sensor based on open magnetizing method and its on-line automated structural health monitoring methodology. Structural Health Monitoring. 2015;**14**(6):583–603

[10] Sun Y, Wu J, Feng B, et al. An opening electric-MFL detector for the NDT of in-service mine hoist wire. IEEE Sensors Journal. 2014;**14**(6):2042–2047

[11] Sun Y, Liu S, Deng Z, et al. Magnetic flux leakage structural health monitoring of concrete rebar using an open electromagnetic excitation technique. Structural Health Monitoring. 2017;**3**:1475921716684340

[12] Zhang W, Li S, Gao F. The modeling and simulations of the circuit element based on finite element methods. In: IEEE International Conference on Vehicular Electronics and Safety, 2005. IEEE; 2005. pp. 257–260

[13] Noreika A, Tarvydas P. Electromagnetic field modeling using edge finite elements. In: BEC 2008. 11th International Biennial Baltic on Electronics Conference, 2008. IEEE; 2008. pp. 99–102

[14] Theory Reference for ANSYS and ANSYS Workbench. ANSYS Release 11.0. SAS IP, Inc.; 2007. p. 1110

[15] Elements Reference. ANSYS Release 11.0. SAS IP, Inc.; 2007. p. 1532

[16] Hirama Y, Takahashi K, Hori S. Electromagnetic inspecting apparatus for magnetizable wire rope: U.S. Patent 4,427,940; 1984-1–24

[17] Katoh M, Masumoto N, Nishio K, et al. Modeling of the yoke-magnetization in MFL-testing by finite elements. NDT & E International. 2003;**36**(7):479–486

[18] Stupakov O, Tomáš I, Kadlecová J. Optimization of single-yoke magnetic testing by surface fields measurement. Journal of Physics D: Applied Physics. 2006;**39**(2):248

[19] Zhang Y, Ye Z, Wang C. A fast method for rectangular crack sizes reconstruction in magnetic flux leakage testing. Ndt & E International. 2009;**42**(5):369–375

[20] Radovanović ID, Rajović NM, Rajović VM, et al. Signal acquisition and processing in the magnetic defectoscopy of steel wire ropes. In: 19th Telecommunications Forum (TELFOR). IEEE; 2011. pp. 864–867

IntechOpen